Efficient prediction of time- and angle-resolved photoemission spectroscopy measurements on a nonequilibrium BCS superconductor

Tianrui Xu, Takahiro Morimoto, Alessandra Lanzara, and Joel E. Moore

Department of Physics, University of California, Berkeley, California 94720, USA
and Materials Sciences Division, Lawrence Berkeley National Laboratory, Berkeley, California 94720, USA

We study how time- and angle-resolved photoemission (tr-ARPES) reveals the dynamics of BCS-type, *s*-wave superconducting systems with time-varying order parameters. Approximate methods are discussed, based on previous approaches to either optical conductivity or quantum dot transport, to enable computationally efficient prediction of photoemission spectra. One use of such predictions is to enable extraction of the underlying order parameter dynamics from experimental data, which is topical given the rapidly growing use of tr-ARPES in studying unconventional superconductivity. The methods considered model the two-time lesser Green's functions with an approximated lesser self-energy that describes relaxation by coupling of the system to two types of baths. The approach primarily used here also takes into consideration the relaxation of the excited states into equilibrium by explicitly including the level-broadening of the retarded and advanced Green's functions. We present equilibrium and nonequilibrium calculations of tr-ARPES spectrum from our model and discuss the signatures of different types of superconducting dynamics.

I. INTRODUCTION

Angle-resolved photoemission spectroscopy (ARPES) is by now well established as a powerful technique to probe the electronic properties of a wide variety of solids [1]. More recently, time-resolved ARPES (tr-ARPES) has been developed as a way to create and measure transient non-equilibrium states of a material that may not appear in its conventional phase diagram [2–4]. In these experiments, an intense pulse "pumps" the system of interest into a nonequilibrium state, followed by a weak "probe." The ejected photo-electrons are then detected with energy and angle resolutions that depend on the time window of the probe pulse. Tr-ARPES measurements can achieve sufficient combined resolution of energy, momentum, and time evolution to study high-T_c superconductors [5–12], in addition to a variety of other materials [13–17].

However, due to the nonequilibrium nature of these experiments, invariance under time translations is broken, with the consequence that one cannot simply analyze and interpret the experimental data through the usual, equilibrium formalism. While general methods that handle nonequilibrium systems, such as the Baym-Kadanoff-Keldysh nonequilibrium quantum field theory [18–20], exist in principle, applying these to predict tr-ARPES spectra that incorporate the transient dynamics of the system as well as the finite duration of the probe pulse is a nontrivial exercise [21–23].

There have been a number of theoretical studies on dynamics of nonequilibrium superconductors [21–47]. An example of the state of the art in numerical simulations of tr-ARPES experiments is Ref. [42], which shows how a sufficiently strong pump coupling to the electrons of a phonon-driven *d*-wave superconductor leads to amplitude (Higgs) mode oscillations at twice the mean gap frequency. That work treats the superconducting gap self-consistently, i.e., changes in

electron distribution induced by the pump modify the superconductivity, and as a result is computationally demanding even for a single pump strength/profile. Here we will not treat the superconducting gap time evolution self-consistently; the goal is that by finding efficient means to compute how different gap evolutions and probe properties would lead to different tr-ARPES signals, our approach can be used to interpret tr-ARPES experimental data and learn how the underlying superconducting gap evolved.

In this respect, our work is more similar to recent theoretical models of a different problem, namely the time-dependent optical conductivity in pump-probe experiments on superconductors. Complementary to work on tr-ARPES, sophisticated nonequilibrium methods have recently been applied to study the transient optical conductivity of nonequilibrium superconducting systems [48,49]. These works were motivated in part by the experimental observation that, in several kinds of superconductors [50], a strong pulse significantly modifies the reflectivity or transmissivity signal that at equilibrium is a standard probe of superconductivity. As the interpretation of these signals in a non-equilibrium context can be subtle [51], a practical nonequilibrium theoretical approach must be developed to extract information from experimental data about the underlying nonequilibrium processes and states, which is a kind of "inverse problem." For example, given data, what is the most likely time dependence of superconductivity to explain the observed results? How does the effective damping depend on system parameters?

That task has been underway for some time in optical conductivity and is here undertaken for tr-ARPES. The main aspect in which our formalism differs from the previous work on optical conductivity in superconductors, aside from being about a different measurement, is in the detailed treatment of

dissipation or level broadening in the system. The importance of dissipation or level broadening can be seen from, for example, considering an idealized probe that suddenly changes ("quenches") the electronic Hamiltonian from a metallic to a superconducting form. In the absence of dissipation, the fact that the metallic ground state is not the ground state of the new Hamiltonian means that some excited states will be occupied. These states would appear as positive-energy states in an tr-ARPES measurement that never dissipate, which does not seem to be what typically happens in reality, where the tr-ARPES intensity above the Fermi level tends to decay as time goes [6–11].

Just as in the theories of pump-probe optical conductivity cited above, adding some form of dissipation is needed if the system is to return to equilibrium eventually. Coupling the system to a "bath" of additional electronic states as in studies of optical conductivity will lead to relaxational time-dependence, but if the bath is finite (as needed for computational purposes) then eventually there will be oscillatory behavior rather than a return of the system to equilibrium. Studying longer times requires larger baths to avoid such oscillations. To prevent nondissipating positive-energy states and/or oscillations, which could exist in tr-ARPES experiments in principle but do not seem to be observed, we adapt a method previously used to incorporate relaxation in the theory of nonequilibrium phenomena in quantum dots [52]. This approach could be viewed as an approximation to a thermodynamically large bath whose treatment is computationally not feasible. We comment in closing on some other possible uses and advantages of this approach.

The specific case treated here is the calculation of the tr-ARPES signal of a BCS s-wave superconducting system with a specified nonequilibrium superconducting order parameter $\Delta(t)$. We use the mean-field (Bogoliubov-de Gennes) approximation to the superconducting system, together with the Keldysh formalism, to tackle the problem. As the approach is also feasible for general momentum and time dependence of the order parameter, it could be easily generalized to superconducting systems other than s-wave. The formalism is computationally efficient enough to be used for the inverse problem, i.e., given an experimental tr-ARPES profile for one or more probe windows, one could compare it to different possible profiles or momentum dependences of the superconducting order parameter.

The rest of the paper is organized as follows. In Sec. II, we review the theory of the tr-ARPES signal, as well as the Keldysh formalism that applies to such calculations. In Sec. II C, we present two approximations to the two-time lesser Green's function, which is the key building block of the tr-ARPES signal, and discuss the assumptions of each approximation. In Sec. III, we show several tr-ARPES calculations with different temporal profiles of BCS order parameters. Finally, we summarize and discuss future directions in Sec. IV.

II. TR-ARPES SIGNAL FROM KELDYSH FORMALISM

In this section, we review the Keldysh formalism applied to the Bogoliubov-de Gennes (BdG) description of a superconductor and the theory of tr-ARPES signals. Then we explain how the lesser Green's function, which is crucial in simulating tr-ARPES signals, is calculated.

A. Keldysh formalism in Bogoliubov-de Gennes (BdG) equation

We first introduce Nambu-spinor notation [53–55]:

$$\Psi_k = (c_{k,\uparrow}, c_{k,\downarrow}, c_{-k,\downarrow}^\dagger, -c_{-k,\uparrow}^\dagger)^T, \tag{1}$$

where $c_{k,\sigma}^\dagger$ creates an electron of momentum k and spin σ. The superscript T denotes transposition. One can then write Green's functions in Eq. (1) basis as follows [19,56,57]:

$$G_{\alpha\beta}^R(t, t') = -i\theta(t - t') \langle \{\Psi_\alpha(t), \Psi_\beta^\dagger(t')\}\rangle,$$

$$G_{\alpha\beta}^A(t, t') = i\theta(t' - t) \langle \{\Psi_\alpha(t), \Psi_\beta^\dagger(t')\}\rangle,$$

$$G_{\alpha\beta}^K(t, t') = -i \langle [\Psi_\alpha(t), \Psi_\beta^\dagger(t')]\rangle,$$

$$G_{\alpha\beta}^<(t, t') = i \langle \Psi_\alpha^\dagger(t')\Psi_\beta(t)\rangle, \tag{2}$$

where R, A, K, and $<$ stand for retarded, advanced, Keldysh, and lesser, and $\langle\cdots\rangle$ is taken with respect to the ground state of the system at zero temperature. The Green's functions are matrices acting on the Nambu spinor basis that are labeled by the indices α, β.

It is straightforward to obtain $G^{R/A}$ when the system is described by a Hamiltonian, $\mathcal{H}$, made of fermion bilinears, as is the case we focus on in this paper. When the Hamiltonian $\mathcal{H}$ is given by

$$\mathcal{H}(t) = \Psi^\dagger H(t)\Psi, \tag{3}$$

where $H(t)$ is the Hamiltonian matrix, $G^{R/A}$ are computed by solving the differential equation [48,56],

$$G^R(t, t) = -i$$

$$i\partial_t G^R(t, t') = H(t)G^R(t, t') \quad t > t' \tag{4}$$

$$G^A(t, t') = [G^R(t', t)]^\dagger.$$

Obtaining $G^{K/<}$ requires solving the Keldysh equation [18] as we explain in the following.

B. TR-ARPES signal from lesser Green's function

Once the lesser Green's function $G^<$ is obtained, the tr-ARPES signal can be calculated from [21]

$$I(k, \omega, t) \propto \text{Im} \int_{t_0}^t dt_1 \int_{t_0}^t dt_2 G_k^<(t_1, t_2)s(t_1)s(t_2)e^{i\omega(t_1 - t_2)}, \tag{5}$$

where $s(t)$ is the temporal profile of the probe pulse, the integration limits, t_0 and t, are controlled by $s(t)$ as the probe pulse has finite width. And we have

$$G_{k,\sigma\sigma'}^<(t_1, t_2) = i \langle c_{k,\sigma}^\dagger(t_2)c_{k,\sigma'}(t_1)\rangle, \tag{6}$$

which is the normal component of the $G^<$ defined in Eqs. (2) with spin indices σ, σ'.

In our calculations for tr-ARPES signals that we show later, we consider systems with spin SU(2) symmetry. In this case, the BdG Hamiltonian [53] is decoupled to two identical 2×2 Hamiltonians spanned by $(c_{k,\uparrow}, c_{-k\downarrow}^\dagger)$ and $(c_{k,\downarrow}, -c_{-k\uparrow}^\dagger)$,

respectively. By focusing on the first one, we can suppress the spin indices in Eq. (6).

C. Lesser Green's function

Now we explain how the lesser Green's function is computed in our framework. We calculate $G^<$ by using Keldysh equation in time domain [58]

$$G^<(t, t') = \int dt_1 \int dt_2 G^R(t, t_1) \Sigma^<(t_1, t_2) G^A(t_2, t'), \quad (7)$$

where all indices but time are suppressed. Here $\Sigma^<$ is the lesser self-energy that effectively determines occupation of electrons in energy eigenstates. Since $G^{R/A}$ are calculated from Eq. (4), one needs to specify the form of the lesser self-energy $\Sigma^<$.

In our framework, we consider the system is coupled to the heat bath with large bandwidth. In this case, we can explicitly write $\Sigma^<$ as [52]

$$\Sigma^<(t_1, t_2) = i\gamma \int \frac{d\omega}{2\pi} f(\omega) e^{-i\omega(t_1-t_2)}$$
$$= \frac{-\gamma/2\pi}{t_1 - t_2 + i0^+}, \quad (8)$$

by integrating out the heat bath, where γ is the level broadening of $G^{R/A}$. This form of self-energy introduces a dissipation effect to the system (with the timescale of $\sim 1/\gamma$) as well as the level broadening of the energy eigenstates ($\sim\gamma$).

Thus we calculate lesser Green's functions via

$$G_k^<(t, t') = \frac{-\gamma}{2\pi} \int dt_1 \int dt_2 \frac{G_k^R(t, t_1) G_k^A(t_2, t')}{t_1 - t_2 + i0^+}$$
$$\times e^{-\gamma(t-t_1+t'-t_2)/2}, \quad (9)$$

where $e^{-\gamma(\cdots)/2}$ is the explicit form of level broadenings of $G^{R/A}$. In the equilibrium systems, Eq. (8) combined with Eq. (7) reproduces the correct form of $G^<(\omega)$ (see Appendix A for detailed derivations) after Fourier transformation.

We note that Ref. [48] used another approximation to calculate $G^<$:

$$G_k^<(t_1, t_2) = i G_k^R(t_1, t_0) n_{0,k} G_k^A(t_0, t_2), \quad (10)$$

where $n_{0,k} = \langle \Psi_k^\dagger \Psi_k \rangle$ at the initial time t_0. In the case of metals, this method gives the correct forms of lesser Green's function, and hence, tr-ARPES spectrum in the equilibrium. It also gives the correct answer for equilibrium superconductors, if we use $n_{0,k}$ that is diagonal in the energy eigenstates of BdG Hamiltonian. However, one major difference between these two formalisms is that a dissipation effect is directly incorporated in Eq. (8), while Eq. (10) gives pure unitary dynamics of time-dependent system (dissipation results from the perspective of one part of the system, which is indeed the microscopic origin of real dissipation).

For example, if we consider a quench problem where a system evolves with

$$H(t) = \theta(-t) H_{\text{metal}} + \theta(t) H_{\text{BCS}}, \quad (11)$$
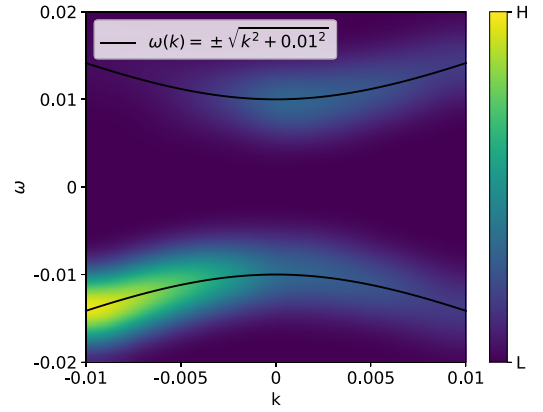

FIG. 1. Nonequilibrium tr-ARPES calculation of constant superconducting gap with a quench, described by Eq. (11) with a BCS superconducting gap $\Delta = 0.01$. The lesser Green's function is calculated using Eq. (10) with $\epsilon_k = k$, $t_p = 500$, $t_0 = 0$, $t = 1000$, $\sigma = 400$. The black curve shows $\omega(k) = \pm\sqrt{k^2 + \Delta^2}$.

there emerges a quenched peak at positive energy, which is shown in Fig. 1 (see Appendix B for details). With Eq. (10), the weight in the positive tr-ARPES peak does not decay due to the absence of dissipation. This coincides with the case of $\gamma \to 0$ in our formalism (see Appendix B for detailed derivations). To incorporate dissipation effects with Eq. (10), one needs to explicitly couple the system to an external bath that dissipates the extra energy [48]. This is physically valid and has the advantage of allowing different microscopic dissipation mechanisms. However, it is computationally advantageous to incorporate dissipation in $\Sigma^<$, so that one does not need to solve time evolution of both the system and the heat bath.

The approach using Eqs. (7) and (8) is used in other areas of nonequilibrium physics and facilitates numerical calculations, especially if the number of bath degrees of freedom is large. As previously mentioned, simulating a heat bath explicitly may lead to unphysical oscillation of expectation values that depends on the system size of the heat bath.

Finally, Eq. (10) is not applicable to interacting systems that involve, for example, four-fermion terms. This can be understood from the absence of dissipation since quasiparticles in interacting systems generally have a finite lifetime. In the formalism using Eqs. (7) and (8), however, extension to interacting systems is straightforward if one uses $G^{R/A}$ and $\Sigma^<$ for the interacting systems in Eq. (7), and incorporates the effect of heat bath by introducing a level broadening to $G^{R/A}$ and the corresponding self-energy of $G^<$.

III. TR-ARPES SIGNAL: CALCULATION

In this section, we show calculations of tr-ARPES signals of systems with different temporal profiles of superconducting order parameter. We start the section by introducing the system that we are considering, both the Hamiltonian of the system as well as the profile of our probe pulse. Then, we provide calculations of: metal, equilibrium BCS, and nonequilibrium BCS systems.

A. Model of 1D superconductor

We consider a BCS-type, s-wave superconducting system with time-varing order parameter:

$$H = \sum_{k,\sigma} \epsilon_k c_{k,\sigma}^\dagger c_{k,\sigma} + \Delta(t) \sum_k c_{k,\uparrow}^\dagger c_{-k,\downarrow} + \text{H.c.}, \quad (12)$$

where $\Delta(t)$ is the *postpump* time-dependent superconducting gap, which is an input to the theory, and is set to be real-valued for now.

We do not consider how $\Delta(t)$ varies due to the time dependence of the pump fields. For ϵ_k, we consider a linear dispersion near fermi surface, i.e., $\epsilon_k = k$.

Note that if the pump field is still on during the probe measurement, one needs to write the lesser Green's function into its gauge-invariant form [23]:

$$G_k^<(t_1, t_2) \rightarrow G_{\tilde{k}}^<(t_1, t_2), \quad (13)$$

by shifting the momentum k via

$$\tilde{k} \rightarrow k + \frac{1}{t_1 - t_2} \int_{-(t_1-t_2)/2}^{(t_1-t_2)/2} dt' A_{\text{pump}}\left(\frac{t_1 + t_2}{2} + t'\right). \quad (14)$$

We rewrite the Hamiltonian Eq. (12) into Nambu-spinor basis:

$$\mathcal{H} = \sum_k \Psi_k^\dagger H_k(t) \Psi_k, \quad (15)$$

where $H_k(t)$ takes the form of

$$H_k(t) = \begin{pmatrix} \epsilon_k & \Delta(t) \\ \Delta(t) & -\epsilon_k \end{pmatrix}. \quad (16)$$

Here we consider 2×2 BdG Hamiltonian spanned by the two-component spinor $\Psi_k = (c_{k,\uparrow}, c_{-k,\downarrow}^\dagger)^T$, by assuming spin SU(2) symmetry.

We thus can solve $G_k^{R/A}$ from

$$G_k^R(t, t) = -i,$$
$$i\partial_t G_k^R(t, t') = H_k(t) G_k^R(t, t') \quad t > t', \quad (17)$$
$$G_k^A(t, t') = \left[G_k^R(t', t)\right]^\dagger.$$

We note two things regarding Eqs. (17). First, the above equations are applicable to the systems that are decoupled in k-space, where the retarded and advanced Green's functions can be solved in each momentum separately. Second, the gap function can be regarded as an anomalous self-energy. In the BCS Hamiltonian that we employ, one assumes an energy-independent order parameter (i.e., a δ function in the time domain), which gives Eqs. (17). In strong coupling regime, on the other hand, the retardation of electron-phonon interaction can be modeled by two-time self-energy, where one needs to solve G^R with the full time dependence of its self-energy.

At the same time, we consider a simple, gaussian probe pulse:

$$s(t) = \frac{1}{\sqrt{2\pi\sigma^2}} e^{-((t-tp)/\sigma)^2}, \quad (18)$$

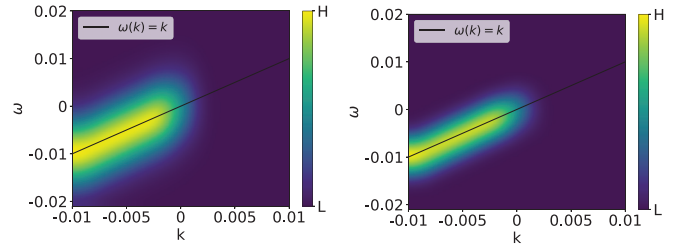where t_p is where the probe pulse centers, and σ tunes the width of the probe pulse.

FIG. 2. Equilibrium tr-ARPES calculations of metal, with $\epsilon_k = k$, $\gamma = 0.0001$, $t_p = 500$, $t = 1000$, $\sigma = 200$ (left panel), $\sigma = 400$ (right panel). The black curve shows $\omega(k) = \epsilon_k$.

B. Equilibrium superconducting system

In this subsection, we demonstrate numerically that tr-ARPES signals in the equilibrium systems are reproduced by our formalism.

We first present calculations of tr-ARPES signal of metals, i.e., $\Delta = 0$ in Eq. (12), from Eq. (5), with both $G^{R/A}$ and $G^<$ calculated numerically via Eqs. (17) and (9).

Figure 2 shows two calculations of tr-ARPES signal of a metal, with numerical solutions to both $G^{R/A}$ from Eqs. (17) and $G^<$ from Eq. (9). The only difference between the two panels is the width of the probe pulse, σ, which determines the energy resolution of the signals, the same as what was mentioned in Ref. [35]. The trend that as σ increases, the width of the tr-ARPES signal decreases, also indicates that as $\sigma \rightarrow \infty$, one may expect [21]

$$I(k, \omega, t) \propto A(k, \omega) f(\omega), \quad (19)$$

where $f(\omega)$ is the Fermi-Dirac distribution at the modeling temperature, in our case, $0K$.

Next, we show tr-ARPES signal of a superconductor.

Figure 3 shows two calculations of tr-ARPES signal of equilibrium BCS superconducting systems with different order parameters. Similar to the metal calculations, the tr-ARPES signal shown here follows $A(k, \omega) f(\omega)$ as expected, up to a broadening of the energy resolution due to finite width of the probe pulse.

C. Nonequilibrium superconducting systems

Last but not least, we present nonequilibrium predictions of tr-ARPES signals with different $\Delta(t)$ profiles as input parameter. We fix the energy resolution by fixing width of the
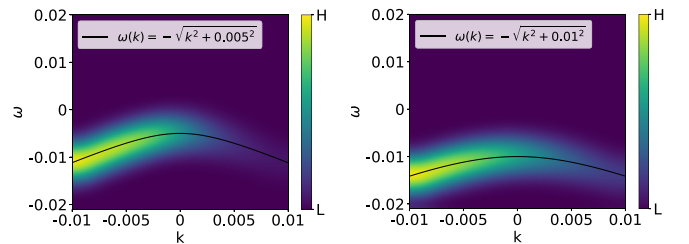

FIG. 3. Equilibrium tr-ARPES calculations of a BCS superconducting system at equilibrium, with $\Delta = 0.005$ (left panel) and $\Delta = 0.01$ (right panel), $\epsilon_k = k$, $\gamma = 0.0001$, $t_p = 500$, $t = 1000$, $\sigma = 400$. The black curve shows $\omega(k) = -\sqrt{\epsilon_k^2 + \Delta^2}$.
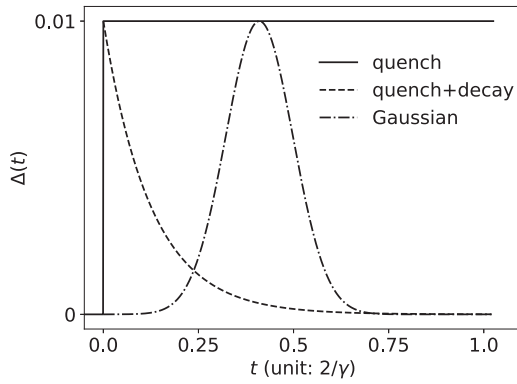
FIG. 4. Schematic plot of various gap profiles considered in this work.

probe pulse, $\sigma = 0.02 \times 2/\gamma$; we vary t_p to probe the system at different times.

We consider the following nonequilibrium gap profiles:

(i) constant order parameter with a quench

$$\Delta(t) = \Delta\theta(t), \qquad (20)$$

(ii) quenched order parameter with decay

$$\Delta(t) = \Delta\theta(t)e^{-t/T}, \qquad (21)$$

(iii) Gaussian order parameter

$$\Delta(t) = \left(\Delta e^{-(\frac{t-t_d}{T})^2} - \Delta_0\right)[\theta(t) - \theta(t - 2t_d)], \qquad (22)$$

where Δ_0 is chosen such that $\Delta(t) = 0$ when $t = 0$ and $t = 2t_d$.

A schematic plot of various $\Delta(t)$'s are shown in Fig. 4. Note that we always turn on nonequilibrium $\Delta(t)$ at $t = 0$ and always consider a system initially at metallic state, i.e., $\Delta(t < 0) \equiv 0$.

1. Constant order parameter with a quench

First, we consider the system with a quenched order parameter, as described by Eq. (20). This situation can be viewed as a sudden opening of a superconducting gap at time $t = 0$, before which the system is metallic. In this situation, we can rewrite H_k as

$$H_k(t) = [1 - \theta(t)]H_{k,\text{metal}} + \theta(t)H_{k,\text{BCS}}, \qquad (23)$$

where $H_{k,\text{metal}}$ takes the form of Eq. (16) with $\Delta(t) = 0$, while $H_{k,\text{BCS}}$ with $\Delta(t) = \Delta$. The resulting tr-ARPES signal as a function of time is shown in Fig. 5. We note that the upper panel of Fig. 5, which shows the tr-ARPES signal at a time right after the quench, resembles Fig. 1. This indicates that the relaxation caused by γ has not yet affected the system at such timescale. However, as time goes, the tr-ARPES signal at positive energies gets relaxed, and eventually, at time of $\sim 2/\gamma$, the signal goes to that described by $H_{k,\text{BCS}}$, as shown in the lower panel of Fig. 5.

We then examine the occupation, n_k, at different k values shortly after the quench:

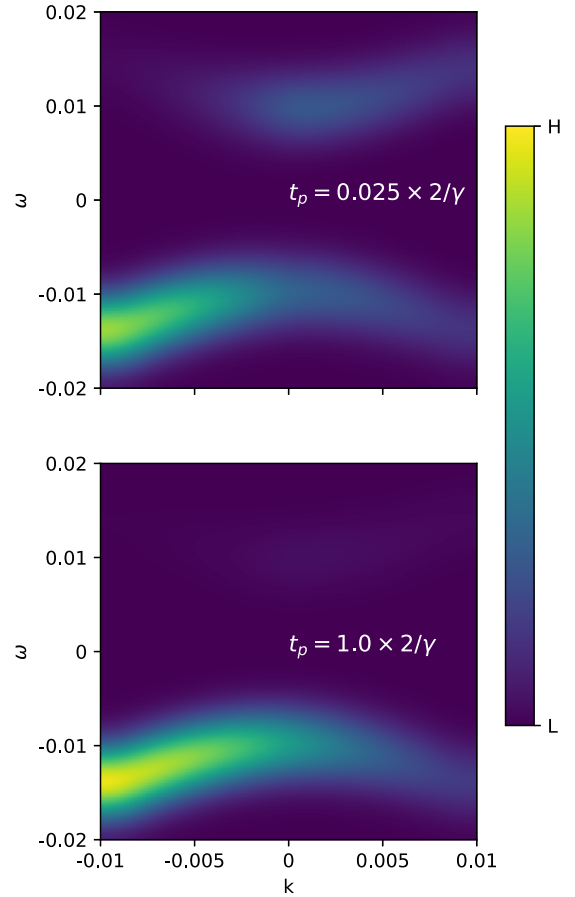$$n_k(t) = \langle c_k^\dagger(t)c_k(t)\rangle = \text{Im}G_k^<(t, t). \qquad (24)$$

FIG. 5. Nonequilibrium tr-ARPES calculations with BCS order parameter featuring constant with a quench, as mentioned in Eq. (20), with $\Delta = 0.01$. The calculation is with $\epsilon_k = k$ and $\gamma = 0.0001$. The width of the probe pulse is $\sigma = 0.02 \times 2/\gamma$. The two different t_p's, short and long time after quench, are indicated in the figures.

$n_k(t)$ is essentially what tr-ARPES measures with a $\delta-$function probe [57].

When t is small, i.e., right after quench, we should expect our system being more *metallic*, namely, all what the quench
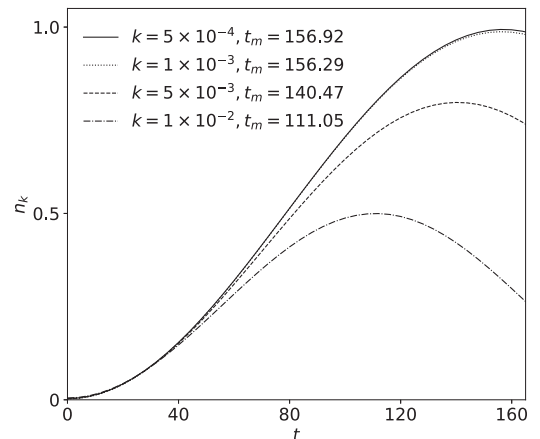

FIG. 6. Occupation number, $n_k(t)$, of the quench system Eq. (20) with $\Delta = 0.01$. The times when n_k peaks, t_m's, are shown in the caption along with their corresponding k values.
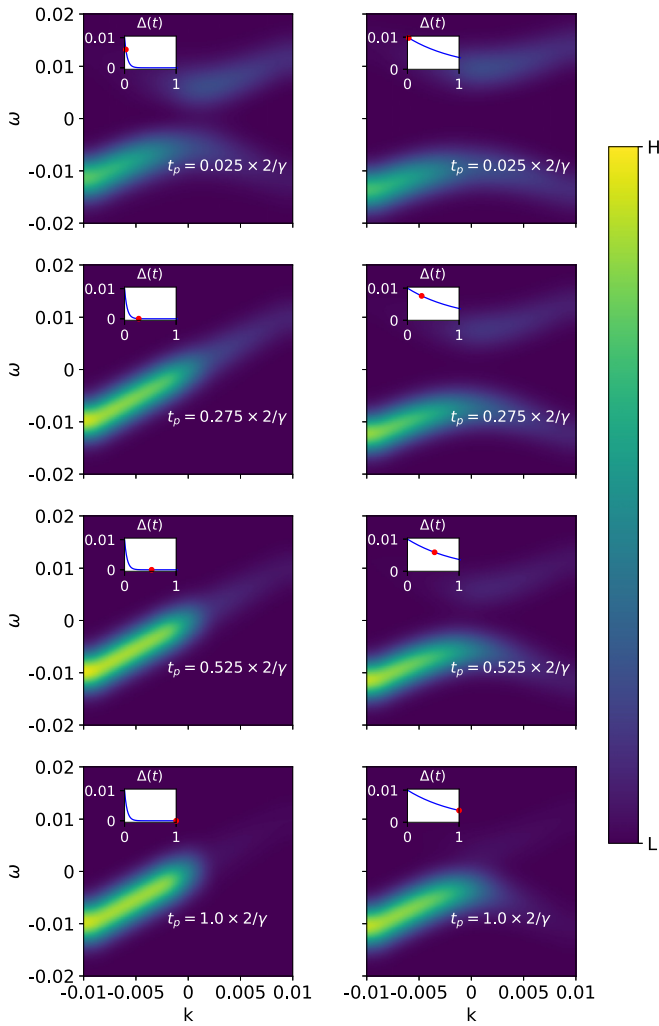
FIG. 7. Nonequilibrium tr-ARPES calculations with BCS order parameters featuring quenched order parameters that decay, as mentioned in Eq. (21), with $\Delta = 0.01$, $T = 0.05 \times 2/\gamma$ (left column) and $1 \times 2/\gamma$ (right column). The calculations are with $\epsilon_k = k$ and $\gamma = 0.0001$. The width of the probe pulse is $\sigma = 0.02 \times 2/\gamma$, and various t_p's are indicated in the figures. The insets of the panels show gap profiles, $\Delta(t)$, as functions of time in unit of $2/\gamma$ in blue curves, and the instantaneous gap at t_p's in red dots.
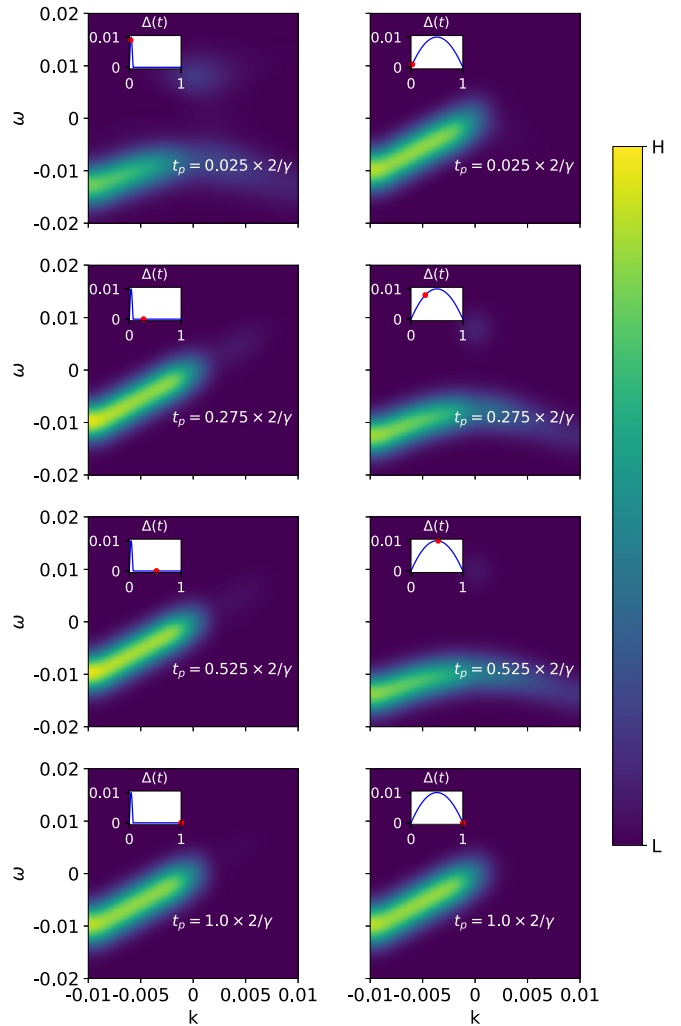
FIG. 8. Nonequilibrium tr-ARPES calculations with BCS order parameters featuring Gaussian order parameters, as mentioned in Eq. (22), with $\Delta(t)_{\max} = 0.01$, $T = 0.05 \times 2/\gamma$ (left column) and $3 \times 2/\gamma$ (right column), $t_d = 0.035 \times 2/\gamma$ (left column) and $0.5 \times 2/\gamma$ (right column). The calculations are with $\epsilon_k = k$ and $\gamma = 0.0001$. The width of the probe pulse is $\sigma = 0.02 \times 2/\gamma$, and various t_p's are indicated in the figures. The insets of the panels show gap profiles, $\Delta(t)$, as functions of time in unit of $2/\gamma$ in blue curves, and the instantaneous gap at t_p's in red dots.

does is projecting the prequench states onto postquench basis. What we should expect for $k > 0$ is that $n_k = 0$ right after the quench, then n_k peaks after some timescale that is defined by $1/E_k$. One should also expect $\lim_{k \to 0^+} n_k \to 1$ at its peak value, since $n_k(t)$ shows Rabi oscillation around its equilibrium value, $1/2$ when $k = 0$, in the postquench system. Figure 6 shows $n_k(t)$ with various k's and $\Delta = 0.01$. We find that the t and k dependence of $n_k(t)$ are as expected, and $n_k(t)$ peaks at time $t_m = \pi/(2E_k)$, with E_k defined in Eq. (A7).

2. Quenched order parameter with decay

Next we consider the the system with a quenched order parameter that decays right after the quench, as described by Eq. (21). We consider two timescales of how fast the order parameter decays: $T \ll 2/\gamma$ and $T = 2/\gamma$. The resulting tr-ARPES signal as a function of time is shown in Fig. 7.

The left column of Fig. 7 shows tr-ARPES of the order parameter that decays with timescale $T \ll 2/\gamma$, while the right column, $T = 2/\gamma$. Comparing left and right columns, one sees similar short-time behavior of tr-ARPES signals but different intermediate- and long-time behaviors. At short-time (the first panels of both columns), both small and large T give signals similar to that of a quench, despite that the signals from small T gives smaller gap than that from large T. For intermediate times (the second and third panels of both columns), the tr-ARPES signals of small and large T show different behaviors: While the large T signals still being gapped and quenchlike, the small T signals becomes gapless, and with a nonzero signal at positive (k, ω). Then, at long time, the tr-ARPES signal of small T seems metallic while that of large T being BCS-like—corresponding qualitatively to their instantaneous BCS gaps.

3. Gaussian order parameter

Finally, we consider the the system with a Gaussian order parameter, as described by Eq. (22). The resulting tr-ARPES signal is shown in Fig. 8.

The left column of Fig. 8 shows tr-ARPES signals of a Gaussian order parameter with $T = 0.05 \times 2/\gamma$ and $t_d = 0.035 \times 2/\gamma$, while the right column shows that with $T = 3 \times 2/\gamma$ and $t_d = 0.5 \times 2/\gamma$. At first glance, the short- and intermediate- time behaviors of tr-ARPES signals (first to third panels of both columns) seem quite different, while the long-time (last panels of both columns) share similarities. However, if we compare the tr-ARPES signals to the instantaneous order parameters at t_p, both columns show tr-ARPES signals that almost follow the instantaneous order parameters, except for a slight quenchlike peak near k_F for the first panel of the left column and the second and third panels of the right column, where the instantaneous order parameters approach the maximum values. In addition, the quenchlike peak is more apparent in the left column than the right column, which may come from that in the left column, the increment of the order parameter is faster than the right column, causing a more significant quenchlike peak at low k. Another feature to notice is that this quenchlike peak only happens near k_F, which is different from an actual quench peak that also extends to $k > k_F$. This may be related to a slower increment of the Gaussian order parameter than that of a sudden quench.

IV. DISCUSSION

The importance of equilibrium ARPES measurements of the electron spectral function to our understanding of unconventional superconductors is clear. To bring tr-ARPES to a similar level of scientific impact, it is necessary to be able to draw conclusions from data about the underlying physics even though what tr-ARPES measures is considerably more challenging to interpret. It is already known from pump-probe studies of optical conductivity and other properties that superconductors support rich nonequilibrium behavior, including significant differences between conventional and unconventional superconductors.

The approach developed here is intended to improve the practical ability of tr-ARPES to probe the nonequilibrium fermionic properties of a complex material. It is worth noting that an implicit assumption we made here is that the pump pulse only affects the system by changing the BCS superconducting gap. However, in actual experiments, the pump field may modify the electron distribution in other ways, where one needs to consider a modified postpump initial state that changes the boundary condition of the lesser Green's function. This can be described by explicitly solving the time-dependent Schrödinger equation with light-matter interaction [35,39,41–44], although that will be more time-consuming. An alternative and more efficient way to approximate this is effectively raising the electron temperature, T_e [59], which is incorporated by increasing the temperature of $\Sigma^<(t, t')$ (see Appendix C for details).

Some obvious extensions to the theory presented here are to non-s-wave superconductors and to incorporate some level of disorder (such as Refs. [46,47,60]), as well as using self-consistently determined BCS order parameters (such as Refs. [49,61,62]) as input to our theory. More challenging extensions would be to approach unconventional superconductivity more microscopically (e.g., via various proposed effective interactions or coupling to order parameters such as nematic or magnetic order) and to compute the superconducting properties of such systems self-consistently, as well as taking other microscopic effect of the pump into consideration, such as stripe melting [63,64] and possible phonon squeezing in K_3C_{60} [50].

But already our nonequilibrium calculations begin to show how various tr-ARPES signals indicate the qualitative differences among order parameter profiles. For example, our calculations show that, a signal at positive (k, ω) indicates that there may be a non-adiabatic change of BCS order parameter (e.g., quenched order parameter); while on the other hand, a time-varying tr-ARPES signal without such peaks may indicate an adiabatic change of BCS order parameter. Other possible ways of using these simulated results include computing and analyzing $\int dk \int_{\omega > 0} d\omega \, I(k, \omega, t)$, and modifying $s(t)$ in Eq. (5) to see how underlying order parameter dynamics may be revealed by different probe pulses. We hope that the model developed here will be useful in the extraction of physics from experimental data, thus indicating constraints for more microscopic theories of superconductivity.

APPENDIX A: DERIVATION OF EQUILIBRIUM $G^<$'S FROM $\Sigma^<$

In this section, we present derivation of equilibrium $G^<$ from $\Sigma^<$ that we proposed in Sec. II C.

To calculate $G^<$ from Eq. (9), one first notices that, due to the causality of G^R and G^A, the explicit integration limits are

$$G_k^<(t, t') = \frac{-\gamma}{2\pi} \int_{-\infty}^{t} dt_1 \int_{-\infty}^{t'} dt_2 \, \frac{G_k^R(t, t_1) G_k^A(t_2, t')}{t_1 - t_2 + i0^+}$$
$$\times e^{-\gamma(t - t_1 + t' - t_2)/2}. \tag{A1}$$

Then, we do the following change of variables:

$$T = \frac{t_1 + t_2}{2},$$
$$\tau = t_1 - t_2, \tag{A2}$$

and thus Eq. (A1) becomes

$$G_k^<(t, t') = \frac{-\gamma}{2\pi} e^{-\gamma(t+t')/2} \int_{-\infty}^{\frac{t+t'}{2}} dT \int_{-\infty}^{\infty} d\tau \frac{G_k^R(t, t_1) G_k^A(t_2, t')}{\tau + i0^+} e^{\gamma T}, \tag{A3}$$

where t_1 and t_2 are functions of T and τ as in Eq. (A2).

Now, let us first plug in $G^{R/A}$ of metal, namely

$$G^R(t, t_1) = -i\theta(t - t_1)e^{-i\epsilon_k(t-t_1)}, \quad G^A(t_2, t') = i\theta(t' - t_2)e^{i\epsilon_k(t'-t_2)}, \tag{A4}$$

then we get $G^<$ of metal from Eq. (A3)

$$G_k^<(t, t') = \frac{-\gamma}{2\pi} e^{-\gamma(t+t')/2} e^{-i\epsilon_k(t-t')} \int_{-\infty}^{\frac{t+t'}{2}} e^{\gamma T} dT \int_{-\infty}^{\infty} \frac{e^{i\epsilon_k\tau}}{\tau + i0^+} d\tau = i\theta(-\epsilon_k)e^{-i\epsilon_k(t-t')}. \tag{A5}$$

At zero temperature, we have $\theta(-\epsilon_k) = f(\epsilon_k)$, thus giving us exactly the $G^<$ one gets via Eqs. (2).

The $G^<$ calculation for BCS superconductor is slightly more complicated, as when one works in Nambu-spinor basis, $G^{R/A}$ becomes a 2×2 matrix:

$$G_k^R(t, t') = \begin{pmatrix} -i[u_k^2 e^{-iE_k(t-t')} + v_k^2 e^{iE_k(t-t')}] & iu_k v_k[e^{iE_k(t-t')} - e^{-iE_k(t-t')}] \\ iu_k v_k[e^{iE_k(t-t')} - e^{-iE_k(t-t')}] & -i[u_k^2 e^{iE_k(t-t')} + v_k^2 e^{-iE_k(t-t')}] \end{pmatrix},$$

$$G_k^A(t, t') = [G^R(t', t)]^\dagger,$$

$$= \begin{pmatrix} i[u_k^2 e^{iE_k(t'-t)} + v_k^2 e^{-iE_k(t'-t)}] & -iu_k v_k[e^{-iE_k(t'-t)} - e^{iE_k(t'-t)}] \\ -iu_k v_k[e^{-iE_k(t'-t)} - e^{iE_k(t'-t)}] & i[u_k^2 e^{-iE_k(t'-t)} + v_k^2 e^{iE_k(t'-t)}] \end{pmatrix}, \tag{A6}$$

with [54]

$$E_k = \sqrt{\epsilon_k^2 + \Delta^2}, \quad u_k^2 = \frac{1}{2}\left(1 + \frac{\epsilon_k}{E_k}\right), \quad v_k^2 = 1 - u_k^2, \tag{A7}$$

Plugging these into Eq. (A3), and doing time-rotation as in Eq. (A2), we get

$$G_k^<(t, t') = \frac{-\gamma}{2\pi} e^{-\gamma(t+t')/2} \int_{-\infty}^{\frac{t+t'}{2}} dT \int_{-\infty}^{\infty} d\tau \frac{u_k^2 e^{-iE_k(t-t'-\tau)} + v_k^2 e^{iE_k(t-t'-\tau)}}{\tau + i0^+} e^{\gamma T}$$

$$= i[u_k^2 \theta(-E_k)e^{-iE_k(t-t')} + v_k^2 \theta(E_k)e^{iE_k(t-t')}]$$

$$= iv_k^2 e^{iE_k(t-t')}, \tag{A8}$$

which is exactly the $G^<$ one gets from direct calculation [Eqs. (2)]. Note that the last equality comes from the fact that E_k is always positive due to its definition in Eq. (A7).

<h2 style="text-align:center">APPENDIX B: THE NONDISSIPATIVE NATURE OF EQ. (10), AND THE $\gamma \to 0$ LIMIT OF EQ. (9)</h2>

To simulate tr-ARPES signal of a quenched system, i.e., Eq. (11), using Eq. (10), one uses G_k^R and G_k^A of the BCS superconducting system that is described by H_{BCS}, i.e., Eq. (A6), while taking $n_{0,k}$ to be that of a metal. Therefore, one gets the quenched lesser Green's function:

$$G_{k,\text{quench}}^<(t, t') = iG_{k,\text{BCS}}^R(t, t_0)\begin{pmatrix} f(\epsilon_k) & 0 \\ 0 & 1 - f(\epsilon_{-k}) \end{pmatrix} G_{k,\text{BCS}}^A(t_0, t'), \tag{B1}$$

Plugging $G_{k,\text{BCS}}^{R/A}$ into the above equation and only taking the normal component, one gets

$$G_{k,\text{quench}}^<(t, t') = if(\epsilon_k)[u_k^4 e^{-iE_k(t-t')} + v_k^4 e^{iE_k(t-t')} + u_k^2 v_k^2 e^{-iE_k(t+t'-2t_0)} + u_k^2 v_k^2 e^{iE_k(t+t'-2t_0)}]$$

$$+ i[1 - f(\epsilon_{-k})]u_k^2 v_k^2[e^{-iE_k(t-t')} + e^{iE_k(t-t')} - e^{-iE_k(t+t'-2t_0)} - e^{iE_k(t+t'-2t_0)}]. \tag{B2}$$

When computing tr-ARPES signal with Eq. (B2), a positive energy peak shows up due to a nonzero value of $u_k^2 v_k^2$. The absence of dissipation prevents such excitation from relaxing.

One can also obtain Eq. (B1) from Eq. (9) by taking $\gamma \to 0$ limit. When γ is small and t, t' are positive but small, one has

$$\int_{-\infty}^t dt_1 \int_{-\infty}^{t'} dt_2 \simeq \int_{-T}^t dt_1 \int_{-T}^{t'} dt_2 \simeq \int_{-T}^0 dt_1 \int_{-T}^0 dt_2 \simeq \int_{-\infty}^0 dt_1 \int_{-\infty}^0 dt_2, \tag{B3}$$

where $T \sim 1/\gamma$ is the effective timescale caused by level broadening of $G^{R/A}$. Then one can approximate $G^<$ with

$$G_k^<(t, t') \simeq \frac{-\gamma}{2\pi} \int_{-\infty}^0 dt_1 \int_{-\infty}^0 dt_2 \frac{G_k^R(t, t_1) G_k^A(t_2, t')}{t_1 - t_2 + i0^+} e^{-\gamma(t-t_1+t'-t_2)/2}. \tag{B4}$$

Now, $G_k^R(t, t')$ and $G_k^A(t, t')$ for the quench problem can be derived analytically by solving the partial differential equation

$$i\partial_t G_k^R(t, t') = H_k(t) G_k^R(t, t'), \tag{B5}$$

with

$$H_k(t) = \theta(-t) H_{k,\text{metal}} + \theta(t) H_{k,\text{BCS}}, \tag{B6}$$

where

$$H_{k,\text{metal}} = \begin{pmatrix} \epsilon_k & 0 \\ 0 & -\epsilon_k \end{pmatrix}, \quad H_{k,\text{BCS}} = \begin{pmatrix} \epsilon_k & \Delta \\ \Delta & -\epsilon_k \end{pmatrix}, \tag{B7}$$

with initial condition $G^R(t', t') = -i$. Let us write $H_{k,\text{metal}} = H_{k,m}$ and $H_{k,\text{BCS}} = H_{k,Sc}$.

The solution to Eq. (B5) is

$$G_k^R(t, t') = \begin{cases} U_1(t, t')(-i) & t' < t < 0 \\ U_2(t, 0) U_1(0, t')(-i) & t' < 0 < t \\ U_2(t, t')(-i) & 0 < t' < t, \end{cases} \tag{B8}$$

where

$$U_{1/2}(t, t') = T\left[\exp\left(-i \int_{t'}^t H_{k,m/Sc} ds\right)\right] = \exp[-i H_{k,m/Sc}(t - t')]. \tag{B9}$$

Then, Eq. (B4) becomes

$$\begin{aligned} G_k^<(t, t') &\simeq -\frac{\gamma}{2\pi} \int_{-\infty}^0 dt_1 \int_{-\infty}^0 dt_2 \frac{U_2(t, 0) U_1(0, t_1)(-i) i U_1^\dagger(0, t_2) U_2^\dagger(t', 0)}{t_1 - t_2 + i0^+} e^{-\gamma(t-t_1+t'-t_2)/2} \\ &= \frac{-\gamma}{2\pi} e^{-\gamma(t+t')/2} U_2(t, 0) \int_{-\infty}^0 dt_1 \int_{-\infty}^0 dt_2 \frac{e^{i H_{k,m}(t_1-t_2)} e^{\gamma(t_1+t_2)/2}}{t_1 - t_2 + i0^+} U_2^\dagger(t', 0) \\ &= i e^{-\gamma(t+t')/2} U_2(t, 0) \begin{pmatrix} f(\epsilon_k) & 0 \\ 0 & f(-\epsilon_k) \end{pmatrix} U_2^\dagger(t', 0) \\ &= i G_{k,\text{BCS}}^R(t, t_0) \begin{pmatrix} f(\epsilon_k) & 0 \\ 0 & f(-\epsilon_k) \end{pmatrix} G_{k,\text{BCS}}^A(t_0, t'), \end{aligned} \tag{B10}$$

with $t_0 = 0$. The last equality holds when $\gamma \to 0$ and t, t' sufficiently small. Also notice that $f(-\epsilon_k) = 1 - f(\epsilon_k) = 1 - f(\epsilon_{-k})$ for system with time-translational invariance.

Hence we have recovered Eq. (B1), the nondissipating limit of the lesser Green's function of a quench BCS system.

APPENDIX C: TR-ARPES SIGNALS WITH THERMAL ELECTRON DISTRIBUTION

The lesser Green's function, with raised temperature, can be calculated using Eq. (7), with

$$\Sigma^<(t_1, t_2, T_e) = i\gamma \int \frac{d\omega}{2\pi} f(\omega, T_e) e^{-i\omega(t_1-t_2)}, \tag{C1}$$

where $f(\omega, T_e)$ is the Fermi-Dirac distribution at temperature T_e. Here we assume that T_e changes much slower than the timescale set by γ, so that this thermal distribution of bath electrons can be considered to be static. This assumption can, in principle, be relaxed by modifying $f(\omega, T_e)$.

With this new $\Sigma^<$, one can describe $G^<$ of electrons whose temperature is increased by the pump field. Such nonzero T_e smears out $I(k, \omega, t)$ in both k and ω directions. We demonstrate this effect by presenting $I(k, \omega, t)$ at a different temperature of three systems: a metallic system ($\Delta = 0$), see Fig. 9; a BCS system ($\Delta = 0.01$), see Fig. 10; and one of the nonequilibrium systems that we have considered in the main text [Eq. (20)], see Fig. 11.

By integrating $I(k, \omega, t)$ over k or ω, we calculate two quantities, $I_\omega(k, t)$ and $I_k(\omega, t)$:

$$I_\omega(k, t) = \int d\omega I(k, \omega, t), \tag{C2}$$

and

$$I_k(\omega, t) = \int dk I(k, \omega, t). \tag{C3}$$

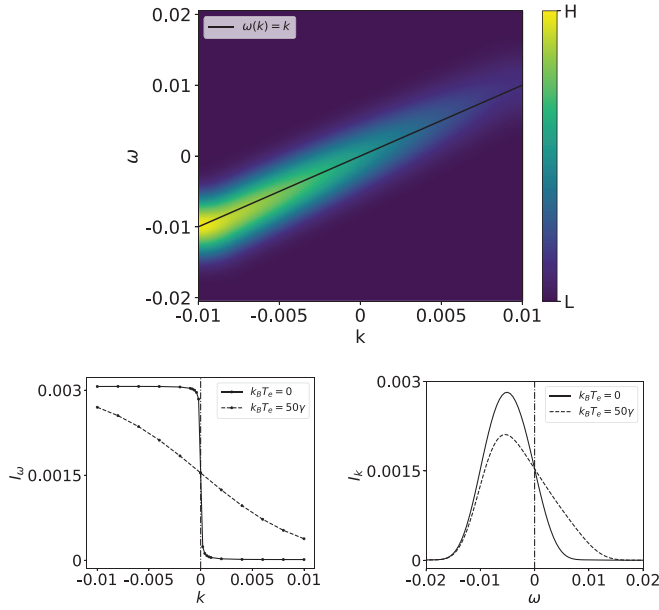These two quantities allow us to directly compare tr-ARPES signals among different temperatures.

FIG. 9. Equilibrium calculations of metal at nonzero temperature: $k_B T_e = 50\gamma$. Upper panel: tr-ARPES signal with $\epsilon_k = k$, $\gamma = 0.0001$, $t_p = 500$, $t = 1000$, $\sigma = 400$. The black curve shows $\omega(k) = \epsilon_k$. Lower panels: $I_\omega(k, t)$ (left) and $I_k(\omega, t)$ (right) at $k_B T_e = 0$ (solid line with dotted data points) and $k_B T_e = 50\gamma$ (dashed line with dotted data points). The vertical dash-dotted lines show where k (left) or ω (right) is zero.
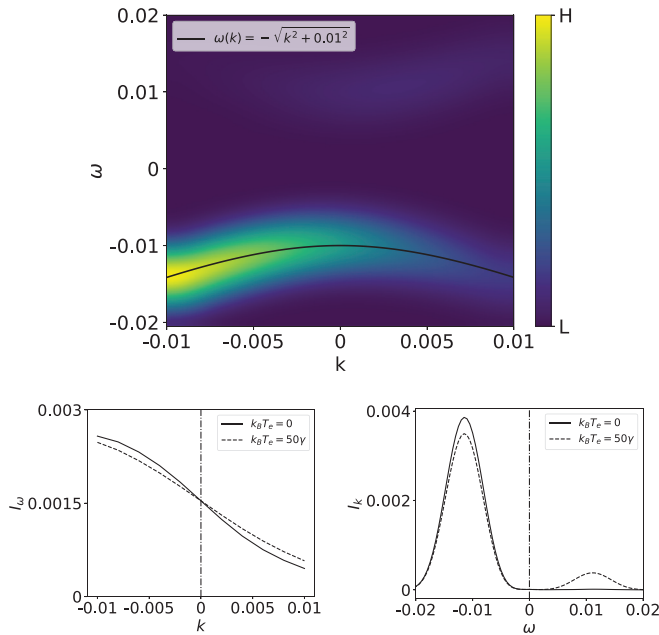

FIG. 10. Equilibrium calculations of a BCS superconducting system with $\Delta = 0.01$ at nonzero temperature: $k_B T_e = 50\gamma$. Upper panel: tr-ARPES signal with $\epsilon_k = k$, $\gamma = 0.0001$, $t_p = 500$, $t = 1000$, $\sigma = 400$. The black curve shows $\omega(k) = -\sqrt{\epsilon_k^2 + \Delta^2}$. Lower panels: $I_\omega(k, t)$ (left) and $I_k(\omega, t)$ (right) at $k_B T_e = 0$ (solid line) and $k_B T_e = 50\gamma$ (dashed line). The vertical dash-dotted lines show where k (left) or ω (right) is zero.
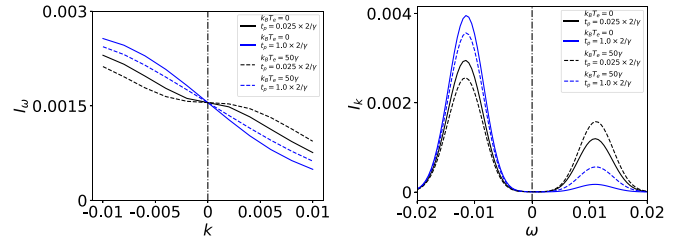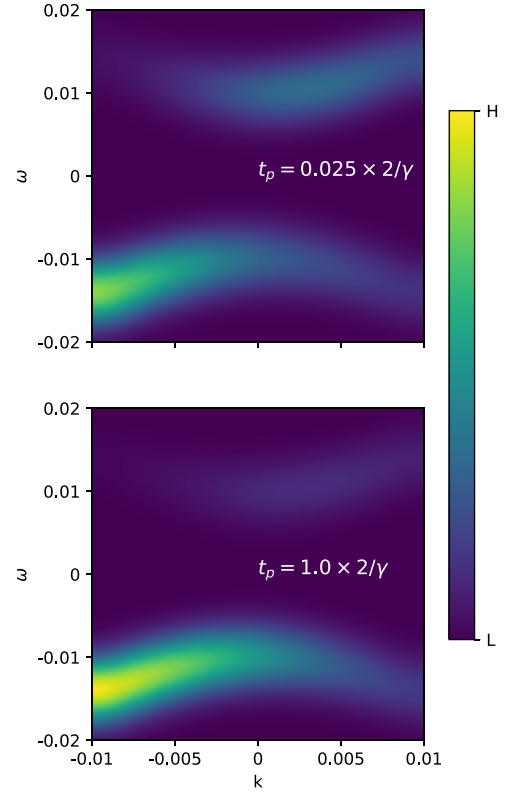

FIG. 11. Nonequilibrium calculations with BCS order parameter featuring constant with a quench, as mentioned in Eq. (20), with $\Delta = 0.01$. Upper panel: tr-ARPES signals with $\epsilon_k = k$, $\gamma = 0.0001$, and $\sigma = 400 = 0.02 \times 2/\gamma$. The two different t_p's, short and long time after quench, are indicated in the figures. Lower panels: $I_\omega(k, t)$ (left) and $I_k(\omega, t)$ (right) at $k_B T_e = 0$ (solid line) and $k_B T_e = 50\gamma$ (dash line), both at short (black line) and long (blue line) time after quench. The vertical dash-dotted lines show where k (left) or ω (right) is zero.

Figures 9 and 10 clearly show that, as temperature increases, the lower energy states are less occupied, while the higher states are more occupied. This happens both in k and ω. On the other hand, Fig. 11 shows that both a nonequilibrium (i.e., time-varying) order parameter and a nonzero T_e may change occupation of the energy states. However, the relaxation introduced by γ eventually causes relaxation of the excitations from nonequilibrium order parameter.

[1] A. Damascelli, Z. Hussain, and Z.-X. Shen, Rev. Mod. Phys. **75**, 473 (2003).

[2] L. Perfetti, P. A. Loukakos, M. Lisowski, U. Bovensiepen, H. Berger, S. Biermann, P. S. Cornaglia, A. Georges, and M. Wolf, Phys. Rev. Lett. **97**, 067402 (2006).

[3] F. Schmitt, P. S. Kirchmann, U. Bovensiepen, R. G. Moore, L. Rettig, M. Krenz, J.-H. Chu, N. Ru, L. Perfetti, D. H. Lu, M. Wolf, I. R. Fisher, and Z.-X. Shen, Science **321**, 1649 (2008).

[4] J. Faure, J. Mauchain, E. Papalazarou, W. Yan, J. Pinon, M. Marsi, and L. Perfetti, Rev. Sci. Instrum. **83**, 043109 (2012).

[5] L. Perfetti, P. A. Loukakos, M. Lisowski, U. Bovensiepen, H. Eisaki, and M. Wolf, Phys. Rev. Lett. **99**, 197001 (2007).

[6] J. Graf, C. Jozwiak, C. L. Smallwood, H. Eisaki, R. A. Kaindl, D.-H. Lee, and A. Lanzara, Nat. Phys. **7**, 805 (2011).

[7] C. L. Smallwood, J. P. Hinton, C. Jozwiak, W. Zhang, J. D. Koralek, H. Eisaki, D.-H. Lee, J. Orenstein, and A. Lanzara, Science **336**, 1137 (2012).

[8] W. Zhang, C. L. Smallwood, C. Jozwiak, T. L. Miller, Y. Yoshida, H. Eisaki, D.-H. Lee, and A. Lanzara, Phys. Rev. B **88**, 245132 (2013).

[9] C. Piovera, Z. Zhang, M. d'Astuto, A. Taleb-Ibrahimi, E. Papalazarou, M. Marsi, Z. Z. Li, H. Raffy, and L. Perfetti, Phys. Rev. B **91**, 224509 (2015).

[10] C. L. Smallwood, W. Zhang, T. L. Miller, G. Affeldt, K. Kurashima, C. Jozwiak, T. Noji, Y. Koike, H. Eisaki, D.-H. Lee, R. A. Kaindl, and A. Lanzara, Phys. Rev. B **92**, 161102 (2015).

[11] S. Parham, H. Li, T. J. Nummy, J. A. Waugh, X. Q. Zhou, J. Griffith, J. Schneeloch, R. D. Zhong, G. D. Gu, and D. S. Dessau, Phys. Rev. X **7**, 041013 (2017).

[12] T. L. Miller, W. Zhang, J. Ma, H. Eisaki, J. E. Moore, and A. Lanzara, Phys. Rev. B **97**, 134517 (2018).

[13] Y. Wang, H. Steinberg, P. Jarillo-Herrero, and N. Gedik, Science **342**, 453 (2013).

[14] F. Mahmood, C.-K. Chan, Z. Alpichshev, D. Gardner, Y. Lee, P. A. Lee, and N. Gedik, Nat. Phys. **12**, 306 (2016).

[15] C. L. Smallwood, R. A. Kaindl, and A. Lanzara, Europhys. Lett. **115**, 27001 (2016).

[16] C. Jozwiak, J. A. Sobota, K. Gotlieb, A. F. Kemper, C. R. Rotundu, R. J. Birgeneau, Z. Hussain, D.-H. Lee, Z.-X. Shen, and A. Lanzara, Nat. Commun. **7**, 13143 (2016).

[17] N. Gedik and I. Vishik, Nat. Phys. **13**, 1029 (2017).

[18] A. Kamenev, *Field Theory of Non-Equilibrium Systems* (Cambridge University Press, Cambridge, 2011).

[19] J. Rammer, *Quantum Field Theory of Non-equilibrium States* (Cambridge University Press, Cambridge, 2007).

[20] M. F. Maghrebi and A. V. Gorshkov, Phys. Rev. B **93**, 014307 (2016).

[21] J. K. Freericks, H. R. Krishnamurthy, and Th. Pruschke, Phys. Rev. Lett. **102**, 136401 (2009).

[22] J. K. Freericks, H. R. Krishnamurthy, and Th. Pruschke, Phys. Rev. Lett. **119**, 189903 (2017).

[23] J. K. Freericks, H. R. Krishnamurthy, M. A. Sentef, and T. P. Devereaux, Phys. Scr. **T165**, 014012 (2015).

[24] A. Rothwarf and B. N. Taylor, Phys. Rev. Lett. **19**, 27 (1967).

[25] A. F. Volkov and Sh. M. Kogan, JETP **38**, 1018 (1974).

[26] A. Schmid and G. Schön, J. Low Temp. Phys. **20**, 207 (1975).

[27] W. H. Parker, Phys. Rev. B **12**, 3667 (1975).

[28] S. B. Kaplan, C. C. Chi, D. N. Langenberg, J. J. Chang, S. Jafarey, and D. J. Scalapino, Phys. Rev. B **14**, 4854 (1976).

[29] S. B. Kaplan, C. C. Chi, D. N. Langenberg, J. J. Chang, S. Jafarey, and D. J. Scalapino, Phys. Rev. B **15**, 3567 (1977).

[30] P. C. Howell, A. Rosch, and P. J. Hirschfeld, Phys. Rev. Lett. **92**, 037003 (2004).

[31] V. M. Axt and T. Kuhn, Rep. Prog. Phys. **67**, 433 (2004).

[32] T. Papenkort, V. M. Axt, and T. Kuhn, Phys. Rev. B **76**, 224522 (2007).

[33] J. Unterhinninghofen, D. Manske, and A. Knorr, Phys. Rev. B **77**, 180509 (2008).

[34] J. Tao and J.-X. Zhu, Phys. Rev. B **81**, 224506 (2010).

[35] M. Sentef, A. F. Kemper, B. Moritz, J. K. Freericks, Z.-X. Shen, and T. P. Devereaux, Phys. Rev. X **3**, 041033 (2013).

[36] A. F. Kemper, M. A. Sentef, B. Moritz, J. K. Freericks, and T. P. Devereaux, Phys. Rev. B **90**, 075126 (2014).

[37] F. Peronaci, M. Schiró, and M. Capone, Phys. Rev. Lett. **115**, 257001 (2015).

[38] S.-L. Yang, J. A. Sobota, D. Leuenberger, Y. He, M. Hashimoto, D. H. Lu, H. Eisaki, P. S. Kirchmann, and Z.-X. Shen, Phys. Rev. Lett. **114**, 247001 (2015).

[39] A. F. Kemper, M. A. Sentef, B. Moritz, J. K. Freericks, and T. P. Devereaux, Phys. Rev. B **92**, 224517 (2015).

[40] C. L. Smallwood, T. L. Miller, W. Zhang, R. A. Kaindl, and A. Lanzara, Phys. Rev. B **93**, 235107 (2016).

[41] M. A. Sentef, A. F. Kemper, A. Georges, and C. Kollath, Phys. Rev. B **93**, 144506 (2016).

[42] B. Nosarzewski, B. Moritz, J. K. Freericks, A. F. Kemper, and T. P. Devereaux, Phys. Rev. B **96**, 184518 (2017).

[43] M. Babadi, M. Knap, I. Martin, G. Refael, and E. Demler, Phys. Rev. B **96**, 014512 (2017).

[44] Y. Murakami, N. Tsuji, M. Eckstein, and P. Werner, Phys. Rev. B **96**, 045125 (2017).

[45] G. Mazza and A. Georges, Phys. Rev. B **96**, 064515 (2017).

[46] Y. Lemonik and A. Mitra, Phys. Rev. B **96**, 104506 (2017).

[47] Y. Lemonik and A. Mitra, Phys. Rev. Lett. **121**, 067001 (2018).

[48] D. M. Kennes, E. Y. Wilner, D. R. Reichman, and A. J. Millis, Phys. Rev. B **96**, 054506 (2017).

[49] D. M. Kennes, E. Y. Wilner, D. R. Reichman, and A. J. Millis, Nat. Phys. **13**, 479 (2017).

[50] M. Mitrano, A. Cantaluppi, D. Nicoletti, S. Kaiser, A. Perucchi, S. Lupi, P. Di Pietro, D. Pontiroli, M. Riccò, S. R. Clark, D. Jaksch, and A. Cavalleri, Nature **530**, 461 (2016).

[51] J. Orenstein and J. S. Dodge, Phys. Rev. B **92**, 134507 (2015).

[52] A.-P. Jauho, N. S. Wingreen, and Y. Meir, Phys. Rev. B **50**, 5528 (1994).

[53] P.-G. de Gennes, *Superconductivity of Metals and Alloys*, Advanced Book Classics (Addison-Wesley Publishing Co., Inc., Redwood City, CA, 1989).

[54] J. Schrieffer, *Theory Of Superconductivity*, Advanced Book Program (The Benjamin/Cummings Publishing Company, Inc., 1964).

[55] L. Fu and C. L. Kane, Phys. Rev. Lett. **100**, 096407 (2008).

[56] J. Rammer and H. Smith, Rev. Mod. Phys. **58**, 323 (1986).

[57] H. Aoki, N. Tsuji, M. Eckstein, M. Kollar, T. Oka, and P. Werner, Rev. Mod. Phys. **86**, 779 (2014).

[58] P. Danielewicz, Ann. Phys. **152**, 239 (1984).

[59] P. B. Allen, Phys. Rev. Lett. **59**, 1460 (1987).

[60] Y. Lemonik and A. Mitra, Phys. Rev. B **98**, 214514 (2018).

[61] R. A. Barankov, L. S. Levitov, and B. Z. Spivak, Phys. Rev. Lett. **93**, 160401 (2004).

[62] Y.-Z. Chou, Y. Liao, and M. S. Foster, Phys. Rev. B **95**, 104507 (2017).

[63] D. Fausti, R. I. Tobey, N. Dean, S. Kaiser, A. Dienst, M. C. Hoffmann, S. Pyon, T. Takayama, H. Takagi, and A. Cavalleri, Science **331**, 189 (2011).

[64] M. Först, R. I. Tobey, H. Bromberger, S. B. Wilkins, V. Khanna, A. D. Caviglia, Y.-D. Chuang, W. S. Lee, W. F. Schlotter, J. J. Turner, M. P. Minitti, O. Krupin, Z. J. Xu, J. S. Wen, G. D. Gu, S. S. Dhesi, A. Cavalleri, and J. P. Hill, Phys. Rev. Lett. **112**, 157002 (2014).